Generalized Hubbard Hamiltonian: Renormalization-group approach

Sergio A. Cannas and Francisco A. Tamarit
Centro Brasileiro de Pesquisas Físicas, Conselho Nacional de Desenvolvimento Científico e Tecnologíco, Rua Xavier Sigaud 150, 22290 Rio de Janeiro, Rio de Janeiro, Brazil and Facultad de Matemática, Astronomía y Física, Universidad Nacional de Córdoba, Laprida 854, 5000 Córdoba, Argentina

Constantino Tsallis
Centro Brasileiro de Pesquisas Físicas, Conselho Nacional de Desenvolvimento Científico e Tecnologíco, Rua Xavier Sigaud 150, 22290 Rio de Janeiro, Rio de Janeiro, Brazil
(Received 5 September 1991)

We study a generalized Hubbard Hamiltonian which is closed within the framework of a quantum real-space renormalization group, which replaces the d-dimensional hypercubic lattice by a diamondlike lattice. The phase diagram of the generalized Hubbard Hamiltonian is analyzed for the half-filled-band case for $d=2$ and $d=3$. Some evidence for superconductivity is presented.

I. INTRODUCTION

The Hubbard model[1] describes a single s band in a tight-binding basis, with local (intrasite) electron-electron interaction. It provides the most simple model to study correlation effects in narrow energy bands, such as metallic magnetism[2] and the metal-insulator transition. It has been often used to describe real materials exhibiting such phenomena.[5] Moreover, in the last years there was an increasing interest in this model and other related ones,[6] mainly because of its applications to the study of high-T_c oxide superconductors.[7–14] In spite of its simplicity, only the one-dimensional case has been solved exactly.[15] Above one dimension different approximate techniques has been applied to obtain partial information about the behavior of the model, both for zero and finite temperature and for various occupations of the band. Among other approximate techniques let us mention mean-field theory,[16] the Green function,[4] variational approaches,[17] and Monte Carlo calculations.[18,19] In particular, for finite temperature, a few works have been done by using a real-space renormalization-group method [for $d=1$ Refs. (20 and 21) and $d=2$ Ref. (22)].

We have recently reported preliminary results on this model by using a quantum real-space renormalization-group (RG) method.[23] Here we discuss the approach in detail and present additional results. Our approximation consists in replacing Bravais lattices by diamondlike hierarchical lattices. This method has proved to be a powerful tool to study critical properties of quantum spin systems.[24,25] In order to apply this RG scheme to the Hubbard Hamiltonian, we derive a new Hamiltonian which generalizes the standard one in such way that it remains invariant under the RG transformation. The present procedure is based on an exact calculation performed for a two-terminal cluster whose iterations yield a hierarchical lattice. It is worthy stressing that the results are not exact for the hierarchical lattice because of the noncommutativity of the involved operators.[25,26] Nevertheless, they are asymptotically exact at high temperature and are believed to be a good approximation for all temperatures. Here we calculate the full $d=2$ and 3 phase diagram for the half-filled-band case.

In Sec. II we briefly review some of the basic properties of the Hubbard Hamiltonian. In Sec. III we discuss the RG formalism and derive the generalized Hamiltonian. A numerical calculation of the phase diagram for the half-filled generalized Hamiltonian is presented for $d=2$ and 3 in Sec. IV. We finally conclude in Sec. V.

II. HUBBARD MODEL

In this section we review some basic properties of the Hubbard Hamiltonian that will be used later on. Let us introduce the dimensionless Hubbard Hamiltonian $\mathcal{H}_H$ defined as follows

$$\begin{aligned}\mathcal{H}_H &\equiv -\beta H_H \\ &= t \sum_{\langle i,j\rangle,\sigma} (c^{\dagger}_{i,\sigma} c_{j,\sigma} + c^{\dagger}_{j,\sigma} c_{i,\sigma}) \\ &\quad - U \sum_i n_{i,\uparrow} n_{i,\downarrow} + \mu \sum_{i,\sigma} n_{i,\sigma} \,, \end{aligned} \tag{1}$$

where $\beta \equiv 1/k_B T$, $c^{\dagger}_{i,\sigma}$ ($c_{i,\sigma}$) is the creation (annihilation) operator for an electron with spin $\sigma=\uparrow,\downarrow$ in a Wannier state centered at the site i of the lattice; $n_{i,\sigma} \equiv c^{\dagger}_{i,\sigma} c_{i,\sigma}$ is the corresponding occupation number; t, U, and μ are, respectively, the dimensionless hopping constant, intrasite electron-electron interaction, and chemical potential; and $\langle i,j\rangle$ runs over all pairs of first-neighboring sites on a d-dimensional hypercubic lattice (with unitary crystalline parameter). The half-filled-band case [i.e., $\langle N\rangle = \mathcal{N}$, where $\mathcal{N}$ is the number of sites of the lattice and $N \equiv \sum_i (n_{i,\uparrow} + n_{i,\downarrow})$] corresponds to $\mu = U/2$. Then (1) takes the form

$$\mathcal{H}_H \equiv -\beta H_H = t \sum_{\langle i,j\rangle,\sigma} (c_{i,\sigma}^\dagger c_{j,\sigma} + c_{j,\sigma}^\dagger c_{i,\sigma}) + \tfrac{1}{2} U \sum_i (n_{i,\uparrow} - n_{i,\downarrow})^2 . \quad (2)$$

As usual, we define the spin operators as

$$S_i^z \equiv n_{i,\uparrow} - n_{i,\downarrow} ,$$
$$S_i^+ \equiv c_{i,\uparrow}^\dagger c_{i,\downarrow} , \quad (3)$$
$$S_i^- \equiv c_{i,\downarrow}^\dagger c_{i,\uparrow} ,$$

and the charge operators as

$$\rho_i^z \equiv n_{i,\uparrow} + n_{i,\downarrow} - 1 ,$$
$$\rho_i^+ \equiv c_{i,\uparrow}^\dagger c_{i,\downarrow}^\dagger , \quad (4)$$
$$\rho_i^- \equiv c_{i,\downarrow} c_{i,\uparrow} .$$

The fermionic character of the c operators imposes the relations

$$(S_i^\nu)^2 + (\rho_i^{\nu'})^2 = 1 ,$$
$$S_i^\nu \rho_i^{\nu'} = S_i^\nu \rho_i^{\nu'} = 0 \quad (\nu, \nu' = x, y, z) , \quad (5)$$

where

$$S_i^x \equiv S_i^+ + S_i^- , \quad \rho_i^x \equiv \rho_i^+ + \rho_i^- ,$$
$$S_i^y \equiv -i(S_i^+ - S_i^-) , \quad \rho_i^y \equiv -i(\rho_i^+ - \rho_i^-) . \quad (6)$$

Let us introduce the unitary transformation[27]

$$c_{i,\downarrow}^\dagger = \exp(i\mathbf{Q}\cdot\mathbf{R}_i) b_{i,\downarrow} , \quad c_{i,\uparrow}^\dagger = b_{i,\uparrow}^\dagger ,$$
$$c_{i,\downarrow} = \exp(-i\mathbf{Q}\cdot\mathbf{R}_i) b_{i,\downarrow}^\dagger , \quad c_{i,\uparrow} = b_{i,\uparrow} , \quad (7)$$

where $\mathbf{Q}$ is the wave vector associated with points which belongs to the corners of the first Brillouin zone [e.g., $\mathbf{Q} = (\pi, \pi, \ldots, \pi)$] such that

$$\exp[i\mathbf{Q}\cdot(\mathbf{R}_i - \mathbf{R}_j)] = \begin{cases} +1 \text{ when } i \text{ and } j \text{ belong to the same sublattice} , \\ -1 \text{ when } i \text{ and } j \text{ belong to different sublattices} , \end{cases}$$

where the hypercubic lattice has been decomposed into two interpenetrating first-neighboring hypercubic sublattices. Consequently, the spin operators S_i^ν are transformed as

$$S_i^+ = \exp(-i\mathbf{Q}\cdot\mathbf{R}_i) \bar{\rho}_i^+ ,$$
$$S_i^z = \bar{\rho}_i^z , \quad (8)$$

where

$$\bar{\rho}_i^+ \equiv b_{i,\uparrow}^\dagger b_{i,\downarrow}^\dagger ,$$
$$\bar{\rho}_i^z \equiv \bar{n}_{i,\uparrow} + \bar{n}_{i,\downarrow} - 1 , \quad (9)$$
$$\bar{n}_{i,\sigma} \equiv b_{i,\sigma}^\dagger b_{i,\sigma} \quad (\sigma = \uparrow, \downarrow) .$$

Also, the charge operators are transformed as

$$\rho_i^+ = \exp(i\mathbf{Q}\cdot\mathbf{R}_i) \bar{S}_i^+ ,$$
$$\rho_i^z = \bar{S}_i^z , \quad (10)$$

where

$$\bar{S}_i^+ \equiv b_{i,\uparrow}^\dagger b_{i,\downarrow} ,$$
$$\bar{S}_i^z \equiv \bar{n}_{i,\uparrow} - \bar{n}_{i,\downarrow} . \quad (11)$$

Applying transformation (7) to the Hamiltonian (2) it is easy to see that $\mathcal{H}_H(t, U) = \overline{\mathcal{H}}_H(t, -U)$, where $\overline{\mathcal{H}}_H$ is obtained from Eq. (2) by replacing the c operators by the b operators. This relation allows a simple mapping of the $U > 0$ region of the phase diagram for the half-filled-band case into the $U < 0$ region. The transformation (7) gives, in fact, a correspondence between charge and magnetic order in such regions (this point will be discussed in detail in Sec. IV B).

We can verify the important properties

$$[\mathcal{H}_H, \mathbf{S}] = 0 , \quad (12)$$
$$[\mathcal{H}_H, N] = 0 , \quad (13)$$

where $\mathbf{S} \equiv \sum_i \mathbf{S}_i$. We now introduce a unitary transformation $\mathcal{U}_\rho$ defined as (see Ref. 28):

$$\mathcal{U}_\rho \equiv \prod_i \exp(i\gamma_i \mathbf{q}_i \cdot \boldsymbol{\rho}_i) , \quad (14)$$

where the $\{\mathbf{q}_i\}$ are arbitrarily chosen unit vectors and the $\{\gamma_i\}$ are parameters of the transformation. If $\mathbf{q}_i = \mathbf{q}$ for every site i and $\mathbf{q}$ lies in the x-y plane, this transformation generalizes the particle-hole exchange transformation.

We want to stress the following important symmetries of the Hamiltonian (2): (a) invariance under $\mathcal{U}_\rho$ when $\mathbf{q}_i = \mathbf{q}$ is in the z direction and $\gamma_i = \gamma$ for all sites i; in this case $\mathcal{U}_\rho$ corresponds to a trivial phase change of the Wannier representation [$\varphi(x) \rightarrow e^{\gamma_i} \varphi(x)$, where $\varphi(x)$ is the Wannier orbital located at site i]; (b) rotational invariance associated with Eq. (12); and (c) invariance under $\mathcal{U}_\rho$ when $\mathbf{q}_i = \mathbf{q}$ lies in the x-y plane, provided that we choose $\gamma_i = -\gamma_j$, where i, j are nearest-neighboring sites (there are cases, for instance frustrated lattices, for which such a choice is not possible). In the non-half-filled-band case, i.e., $\mu \neq U/2$, the Hamiltonian (1) loses symmetry (c), but it still preserves symmetries (a) and (b). Let us mention here another symmetry [noted as (d)] which is satisfied neither by Hamiltonian (1) nor (2), but which we shall use later on: (d) invariance under $\mathcal{U}_\rho$ with $\mathbf{q}$ in the x-y plane and $\gamma_i = \gamma$ for all sites i.

III. RENORMALIZATION GROUP

In order to study the thermodynamics of the model, at least as far as criticality is concerned, we can use real-

space renormalization-group approaches. For instance, the lattice could be divided in two sublattices A and B. Then we can define, by decimating the B sublattice, a Hamiltonian $\mathcal{H}'$ on A which satisfies

$$\exp(\mathcal{H}'+\mathcal{C})=\mathrm{Tr}_B[\exp(\mathcal{H})] , \tag{15}$$

where $\mathcal{H}$ is given by (2) and where Tr_B represents a partial trace over all the degrees of freedom associated to sites of the sublattice B. As is well known, the decimation transformation defined by Eq. (15) cannot be carried out exactly on a Bravais lattice. This is due either to the *infinite* proliferation of couplings constants through successive decimations or to the noncommutativity among the various terms of the Hamiltonian. In order to avoid the infinite coupling proliferation, we use a quantum real-space renormalization-group (RG) method in which the Bravais lattices are replaced by diamondlike hierarchical lattices, namely, those associated with the clusters shown in Fig. 1. Such lattices are defined through infinite iterations of a two-rooted cluster which consists in an array of b^{d-1} strings in parallel, each string being constituted by b bonds in series. Then the hierarchical lattice contains an infinite number of clusters such as those of Fig. 1. With each of these clusters, a Hamiltonian (denoted by $\mathcal{H}_k$) can be associated. Consequently, the total Hamiltonian can be expressed as

$$\mathcal{H}=\sum_k \mathcal{H}_k . \tag{16}$$

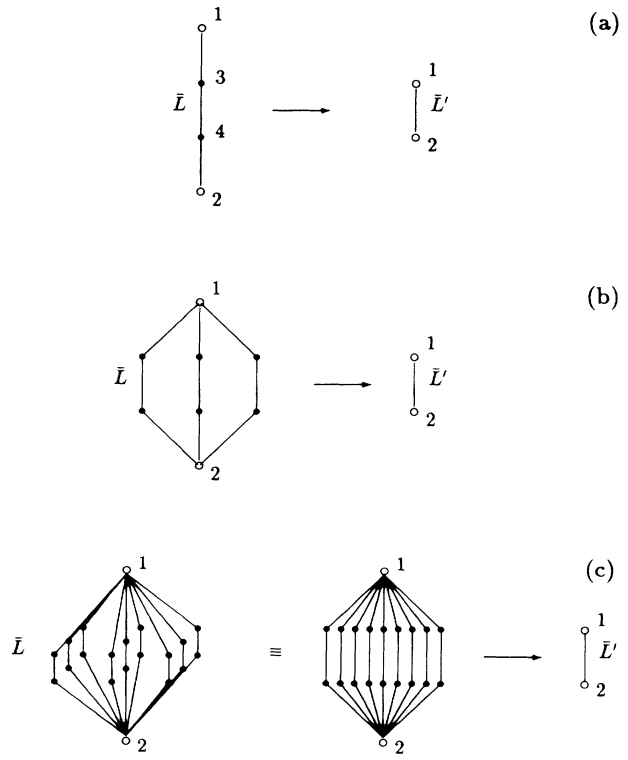

FIG. 1. Renormalization-group cell transformation. $\bar{L}$ stands for the set of parameters of the Hamiltonian [e.g., (U,t,μ) for $\mathcal{H}_H$]. (a) $d=1$, (b) $d=2$, and (c) $d=3$.

For classical systems it is, of course, true that $\exp(\mathcal{H})=\prod_k \exp(\mathcal{H}_k)$, and therefore, if $\mathcal{H}_k$ is exactly tractable, the present approach will enable the exact solution of the hierarchical lattice. This is not so for a quantum system because of noncommutativity. We then work within the approximation

$$\exp\left[\sum_k \mathcal{H}_k\right]\approx\prod_k \exp(\mathcal{H}_k) . \tag{17}$$

This equation reduces the problem to the proper renormalization of a finite (relatively small) cluster. It is clear that Eq. (17) becomes asymptotically exact in the $T\to\infty$ limit, even if the problem is a quantum one[26] (this fact has already been verified for the Hubbard model[21] and for spin models[25]). It is, or course, possible in principle to work within approximations systematically better than Eq. (17), but this is not the aim of the present work. It is worthy to mention also that the present procedure is believed to preserve the two-body correlation function (this is already proved for the classical case).[29] To perform the renormalization within the present scheme, we would like to satisfy

$$\exp(\mathcal{H}'_k+C)=\mathrm{Tr}_{\text{internal sites}}[\exp(\mathcal{H}_k)] , \tag{18}$$

where $\mathcal{H}_k$ denotes the Hamiltonian associated to the cluster under consideration and $\mathcal{H}'_k$ denotes the renormalized Hamiltonian of the two-site chain (see Fig. 1). In fact, this is not possible for the Hamiltonian (2). Indeed, if $\mathcal{H}_k$ is the standard Hubbard Hamiltonian, proliferation occurs and the resulting $\mathcal{H}'_k$ contains new terms that were not present in $\mathcal{H}_k$; however, the proliferation does not go indefinitely, and a generalized Hamiltonian exists which contains a *finite* number of terms and which *exactly* satisfies Eq. (18). Therefore we have to search for a generalization of the Hubbard Hamiltonian (2) which might satisfy this relation. As we shall see, the form of the new Hamiltonian depends strongly on the choice of the cluster. Some choices yield a new Hamiltonian which does not reproduce all the symmetries of the Hubbard Hamiltonian; in such situation the extended Hamiltonian will not recover the initial one as a particular case. Therefore our next task is to choose a suitable cluster. For simplicity let us start by considering the one-dimensional case. We ask for the smallest one-dimensional cluster for which the decimation transformation (18) preserves all the Hubbard Hamiltonian symmetries we are interested in [namely, symmetries (a), (b), and (c) of Sec. II]. If a three-site cluster was used, the resulting Hamiltonian through Eq. (18) would satisfy symmetries (a) and (b) but not (c); it would instead satisfy (d). Clearly, this Hamiltonian *will not contain* the original Hubbard Hamiltonian as a particular case. In order to avoid this inconvenience, we choose a four-site cluster, for which the resulting Hamiltonian through Eq. (18) satisfies all symmetries (a), (b), and (c). To be more explicit, if we attribute alternating γ and $-\gamma$ for each site of the chain, the four-site cluster leaves under decimation $\gamma_1=+\gamma$ and $\gamma_2=-\gamma$ for the two-site renormalized cluster [see Fig. 1(a)], whereas the three-site cluster yields

$\gamma_1=\gamma_2=+\gamma$. The above argument not only applies to a linear chain, but to all two-terminal clusters whose topology enables them to satisfy the invariance property (c). The cluster used by Castellani *et al.*[28] is the three-site one and, consequently, suffers from this inconvenience. This point is rather subtle and will hopefully become clear through the discussion of a sequence of extensions of Hamiltonian (1).

The next step is then to find a generalized half-filled-band Hamiltonian [denote by $\mathcal{H}_G$ Ref. (23)] which extends Hamiltonian (2) while preserving symmetries (a), (b), and (c). By following along the lines introduced in Ref. 28, we obtain the structure of $\mathcal{H}_G$ without explicitly performing the calculations involved in Eq. (18). More precisely, we look for *all* the one- and two-site operators which satisfy the just mentioned symmetries: A linear combination of such terms yields the desired Hamiltonian, namely,

$$\mathcal{H}_G=t\sum_{\langle i,j\rangle,\sigma}(c_{i,\sigma}^{\dagger}c_{j,\sigma}+c_{j,\sigma}^{\dagger}c_{i,\sigma})+\tfrac{1}{2}U\sum_i(S_i^z)^2-J\sum_{\langle i,j\rangle}\mathbf{S}_i\cdot\mathbf{S}_j-K\sum_{\langle i,j\rangle}(S_i^z)^2(S_j^z)^2$$
$$-I\sum_{\langle i,j\rangle}[\rho_i^z\rho_j^z-(\rho_i^x\rho_j^x+\rho_i^y\rho_j^y)]+D\sum_{\langle i,j\rangle,\sigma}(c_{i,\sigma}^{\dagger}c_{j,\sigma}+c_{j,\sigma}^{\dagger}c_{i,\sigma})(n_{i,-\sigma}-n_{j,-\sigma})^2\ . \tag{19}$$

This is the *minimal* Hamiltonian which satisfies Eq. (18) and contains Hamiltonian (2) as a particular case. It is worthy to point out here that, although we have followed the method introduced by Castellani *et al.*, our generalized Hamiltonian is not the same they found. As already mentioned, this difference is due to the different clusters they and we have used.

We note the following properties.

(i) For $J=K=I=D=0$, we recover the half-filled-band Hubbard Hamiltonian (2), as expected.

(ii) If we use the transformation (14) with $\mathbf{q}_i=\mathbf{q}$ for all sites i, $\mathbf{q}$ being along the z direction and $(\gamma_i-\gamma_j)=\pi$ (i,j nearest-neighbor sites), we can show that the grand partition function $Z=\mathrm{Tr}\exp(\mathcal{H}_G^{\mu})$ associated with the Hamiltonian (19) satisfies $Z(t,D)=Z(-t,-D)$. This point greatly generalizes the one established in Ref. 28.

(iii) Using the standard particle-hole exchange transformation, it can be shown that Hamiltonian (19) preserves the half-filled-band character of (2).

(iv) Applying the transformation (7), it can be seen that the Hamiltonian (19) is transformed as

$$\mathcal{H}_G(U,K,J,I,t,D)\rightarrow\overline{\mathcal{H}}_G(2(zK-\tfrac{1}{2}U),K,I,J,t,D)\ , \tag{20}$$

where z equals the coordination number of a Bravais lattice and equals 2 for the simple hierarchical lattices we are using here; $\overline{\mathcal{H}}_G$ is obtained from $\mathcal{H}_G$ by replacing the c operators by the b operators [see Eqs. (7)–(11)]. Consequently, for $K=U/2$ and $J=I$, the Hamiltonian (19) remains invariant under transformation (7). We can verify that this symmetry is preserved by Eq. (18); consequently, the subspace $(K,J)=(U/2,I)$ is invariant under the RG transformation in the (U,K,J,I,t,D) parameter space.

(v) For $t=D=I=0$, the Hamiltonian (19) becomes a simple J-K-U model characterized by the Hamiltonian

$$\mathcal{H}_{J\text{-}K\text{-}U}=-J\sum_{\langle i,j\rangle}\mathbf{S}_i\cdot\mathbf{S}_j-K\sum_{\langle i,j\rangle}(S_i^z)^2(S_j^z)^2+\tfrac{1}{2}U\sum_i(S_i^z)^2 \tag{21}$$

This Hamiltonian looks like a quantum analog of the Blume-Emery-Griffiths (BEG) Hamiltonian.[30,31] In fact the situation is more complex than that. This is due to the fact that the $\mathbf{S}_i$ operators cannot be interpreted as standard spin-1 operators (see Ref. 28). It can be seen that $\mathcal{H}_{J\text{-}K\text{-}U}$ satisfies symmetries (a), (b), (c), and (d) mentioned above. Therefore it also constitutes an invariant subspace under the RG transformation.

(vi) The $J=0$ case of $\mathcal{H}_{J\text{-}K\text{-}U}$ is isomorphic to the spin-$\frac{1}{2}$ Ising model in the presence of an external field. Indeed, by defining a new variable[33]

$$t_i\equiv 2(S_i^z)^2-1\ ,\quad t_i=\pm 1\ , \tag{22}$$

and by taking into account the double degeneracy of the $S_i^z=0$ states, $\mathcal{H}_{J\text{-}K\text{-}U}$ equals $(K/4)\sum_{\langle i,j\rangle}t_it_j+H_t\sum_i t_i$, where

$$H_t=\tfrac{1}{2}(\tfrac{1}{2}U-K)\ . \tag{23}$$

$J=0$ constitutes an invariant subspace under the RG transformation; it contains an even smaller subspace, namely, $K=U/2$, i.e., $H_t=0$.

Let us now focus on the case of non-half-filled band. As we have seen in Sec. II, the Hamiltonian (1) does not have symmetry (c). By repeating the procedure which leads us from Hamiltonian (2) to Hamiltonian (19), we can now generalize Hamiltonian (1) by only demanding the preservation of symmetries (a) and (b). We obtain

$$\mathcal{H}_G^{\mu}=t\sum_{\langle i,j\rangle,\sigma}(c_{i,\sigma}^{\dagger}c_{j,\sigma}+c_{j,\sigma}^{\dagger}c_{i,\sigma})+\tfrac{1}{2}U\sum_i(S_i^z)^2+\tilde{\mu}\sum_{i,\sigma}n_{i,\sigma}-J\sum_{\langle i,j\rangle}\mathbf{S}_i\cdot\mathbf{S}_j-K\sum_{\langle i,j\rangle}(S_i^z)^2(S_j^z)^2$$
$$+Y\sum_{\langle i,j\rangle}\boldsymbol{\rho}_i\cdot\boldsymbol{\rho}_j-I\sum_{\langle i,j\rangle}[\rho_i^z\rho_j^z-(\rho_i^x\rho_j^x+\rho_i^y\rho_j^y)]+R\sum_{\langle i,j\rangle}[(\rho_i^z)^2\rho_j^z+(\rho_j^z)^2\rho_i^z]$$
$$+D\sum_{\langle i,j\rangle,\sigma}(c_{i,\sigma}^{\dagger}c_{j,\sigma}+c_{j,\sigma}^{\dagger}c_{i,\sigma})(n_{i,-\sigma}-n_{j,-\sigma})^2+E\sum_{\langle i,j\rangle,\sigma}(c_{i,\sigma}^{\dagger}c_{j,\sigma}+c_{j,\sigma}^{\dagger}c_{i,\sigma})n_{i,-\sigma}n_{j,-\sigma}\ , \tag{24}$$

where $\tilde{\mu}=\mu-U/2$. This Hamiltonian contains the following models as particular cases.

(i) For $J=K=I=Y=R=D=E=0$, we recover the standard Hubbard model (1).

(ii) For $\tilde{\mu}=R=E=Y=0$, we recover Hamiltonian (19).[23]

(iii) For $\tilde{\mu}=R=I=0$, $D=-t$, and $E=2D$, we precisely recover the Hamiltonian (here denoted by $\mathcal{H}_{\rm CD}$) obtained by Castellani *et al.*[28] for the three-site cluster and half-filled band. Hamiltonian $\mathcal{H}_{\rm CD}$ satisfies symmetries (a), (b), and (d) [whereas Hamiltonian $\mathcal{H}_G$ satisfies symmetries (a), (b), and (c)].

(iv) For $K=R=I=Y=0$, $D=E=-t$, and taking the limit $U\to\infty$ while keeping μ finite, we obtain the t-J model.[6,7] A generalized version of this model will be discussed elsewhere.

(v) For $K=I=Y=R=D=E=0$, we obtain the Hubbard-Heisenberg model.[32]

Next, we consider the non-half-filled-band model with an external magnetic field B in the z direction. In this case the symmetry (b) must be replaced by the more restricted one $[\mathcal{H}_H,S^z]=0$. By following the same procedure as before, we obtain that the Hamiltonian which is invariant under the RG transformation is

$$\mathcal{H}_G^{\mu B}=\mathcal{H}_G^{\mu}+\mathcal{H}_B\ , \tag{25}$$

where

$$\mathcal{H}_B=B\sum_i S_i^z-J_2\sum_{\langle i,j\rangle}[S_i^zS_j^z-(S_i^xS_j^x+S_i^yS_j^y)] +R_2\sum_{\langle i,j\rangle}[(S_i^z)^2S_j^z+(S_j^z)^2S_i^z]\ . \tag{26}$$

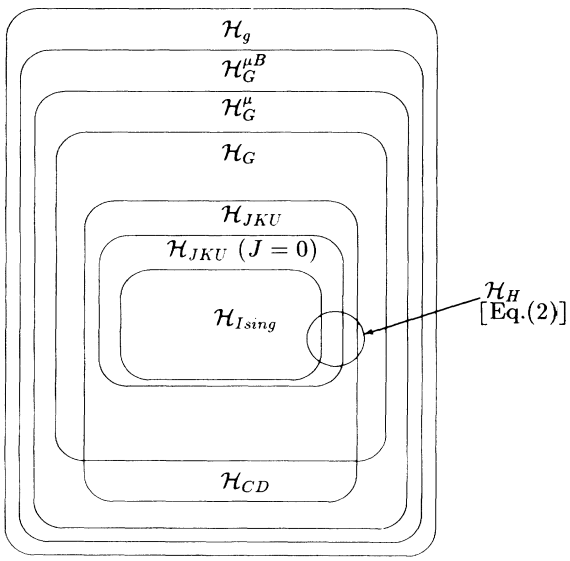

FIG. 2. Hierarchical sequence of the present Hamiltonians. The rectangular blocks refer to sequences of *symmetries* (which do not always coincide with sequences of particular values of $\mathcal{H}_g$). The circle indicates the position of the Hubbard Hamiltonian $\mathcal{H}_H$ [Eq. (2)]; note that it is contained in $\mathcal{H}_G$ but not in $\mathcal{H}_{\rm CD}$.

If we consider $B=R=R_2=\tilde{\mu}=t=D=E=I=Y=0$ and $U\to\infty$, $\mathcal{H}_G^{\mu B}$ becomes the spin-$\frac{1}{2}$ anisotropic Heisenberg Hamiltonian, which in turns contains, for $J_2=0$, the isotropic Heisenberg model as a particular case.

Finally, the most general one- and two-body single-band fermionic Hamiltonian $\mathcal{H}_g$ can be obtained as a generalization of the Hamiltonian $\mathcal{H}_G^{\mu B}$. Such Hamiltonian will satisfy in principle none of the above-mentioned symmetries. The general form of $\mathcal{H}_g$ can be obtained by the same procedure used to generate the sequence of Hamiltonians we have analyzed. For instance, the term

$$Y\sum_{\langle i,j\rangle}\boldsymbol{\rho}_i\cdot\boldsymbol{\rho}_j-I\sum_{\langle i,j\rangle}[\rho_i^z\rho_j^z-(\rho_i^x\rho_j^x+\rho_i^y\rho_j^y)]\ ,$$

in Hamiltonian (24), will be replaced by the more general one

$$\sum_{\langle i,j\rangle}(I_z\rho_i^z\rho_j^z+I_x\rho_i^x\rho_j^x+I_y\rho_i^y\rho_j^y)\ .$$

The complete sequence of symmetries we have analyzed in this section is summarized in Fig. 2.

IV. PHASE DIAGRAM: HALF-FILLED-BAND CASE

In this section we calculate numerically the phase diagram of the generalized Hamiltonian for the half-filled-band case (19). The RG recurrence equations are obtained by explicitly computing the partial trace

$$\exp(\mathcal{H}'_G+\mathcal{C})=\operatorname*{Tr}_{\text{internal sites}}[\exp(\mathcal{H}_G)]\ , \tag{27}$$

where $\mathcal{H}_G$ denotes the generalized Hamiltonian associated with the cluster being considered and $\mathcal{H}'_G$ denotes the renormalized Hamiltonian of the two-site chain (see Fig. 1). Let us first consider the $d=1$ four-site cluster [Fig. 1(a)]. In this case the partial trace (27) is calculated by summing the matrix elements of $\exp(\mathcal{H}_G)$ over the set of occupation numbers $\{n_{3,\sigma},n_{4,\sigma}\}$. In order to compute such matrix elements, we must diagonalize $\mathcal{H}_G$. The Fock space $|\{n_{i,\sigma}\}\rangle$ associated with the four-site chain is of dimension 2^8; in such space $\mathcal{H}_G$ is represented by a 256×256 matrix. As we have seen, the total number of particles and z component of the total spin are good quantum numbers for this problem [Eqs. (12) and (13)]. So, using the fact that the basis vectors are simultaneously eigenvectors of N and S^z, we can present $\mathcal{H}_G$ in a block-diagonal structure by simply rearranging the order of these vectors according to the eigenvalues of N and S^z. The largest block (corresponding to the eigenvalues $N=4$, $S^z=0$) is a 36×36 matrix. It is possible to further reduce the size of the blocks by using some supplementary symmetries. However, the blocks do not become small enough to be analytically tractable. So we have not performed this further reduction, and excepting for a few special cases, the calculation has been done numerically. Using Eq. (27), we obtain the recurrence relations between the set of parameters $\bar{L}\equiv(U,K,J,I,t,D)$ of $\mathcal{H}_G$ and the set of renormalized parameters $\bar{L}'\equiv(U',J',K',I',t',D')$ of $\mathcal{H}'_G$:

$$\bar{L}' = \bar{L}'_1(\bar{L}) , \tag{28}$$

where the subindex 1 stands for $d=1$. In order properly to take into account the weights of the single-site terms, we associated U with every internal site and $U/2$ with each of the two-terminal sites.

Now consider a more general diamondlike cluster of the type shown in Figs. 1(a), 1(b), and 1(c). The fractal dimensionalities d_f of the hierarchical lattices generated by these clusters, respectively, are $d_f = \ln 3/\ln 3 = 1$, $d_f = \ln 9/\ln 3 = 2$, and $d_f = \ln 27/\ln 3 = 3$, and hence, in general, $d_f = d$. Every cluster of this kind consists in a parallel array of 3^{d-1} four-site chains, and so the corresponding Hamiltonian is given by the sum of linear-chain Hamiltonians. Therefore, within the approximation indicated in Eq. (17), we obtain

$$\bar{L}' = \bar{L}'_d(\bar{L}) = b^{d-1}\bar{L}'_1(\bar{L}) , \tag{29}$$

where $b=3$ is the length scale of the RG transformation. Using Eq. (29), we analyzed the RG flow in the parameter space (U,K,J,I,t,D) for $d=1$, 2, and 3. This flow provides the corresponding phase diagram. We have numerically studied the most relevant sections of this complex phase diagram. Most of the attractors (fully stable fixed points) and many of the relevant fixed points (semistable or fully unstable) are located at the invariant subspace $t=D=0$, which has been analyzed in Secs. IV A and IV B. The $t\neq 0$ region has been explored in Secs. IV C and IV D. Most of the $D\neq 0$ region is driven, under the RG transformation, onto the $D=0$ case; consequently, no critical novelties are expected in the $D\neq 0$ region. The few exceptions which are observed are discussed in Secs. IV C and IV D.

A. J-K-U model ($I=t=D=0$)

We now consider the section $I=t=D=0$ of the full phase diagram; i.e., we analyze the phase diagram associated with the Hamiltonian (21) (we recall this Hamiltonian is closed under the RG transformation). We are mainly interested in the antiferromagnetic case ($J>0$), because its fixed-point structure determines to some extent the Hubbard model phase diagram (see Sec. IV C). The ferromagnetic case ($J<0$) presents results which are analogous to those of the $J>0$ one. More precisely, to each fixed point at $J>0$, it is associated a similar one at $J<0$, which exhibits the same stability; in fact, this is true for the entire RG flow topology. Therefore it suffices to consider the $J\geq 0$ case. The analogy between the $J>0$ and $J<0$ cases is physically expected, and it is correctly reproduced by the present RG because of the *odd* number of bonds appearing in all minimal paths between the two terminals of the clusters we are using. It is worthy mentioning that the RG recurrence equations for the J-K-U model have been analytically obtained.

First of all, we shall treat the invariant subspace $J=0$. Note that in this case flipping any spin ($S_i^z \rightarrow -S_i^z$) does not change the energy of an arbitrary configuration, and so the (spontaneous) magnetization is zero for $J=0$. The line $K=U/2$ corresponds to $H_t=0$ [see Eq. (23)] and therefore also constitutes an invariant subspace. In some sense it is a symmetry line of the phase diagram, since the RG flow is topologically equivalent on both sides of it. The relationship of this symmetry with the complete Hamiltonian (19) was already pointed out in Eq. (20). The flow diagram in the (U,K) plane is shown in Fig. 3 for $d=2$ (the $d=3$ flow diagram is completely analog). Along the line $K=U/2$, we find two fully unstable fixed points labeled a, a', in Fig. 2. We find three fully stable fixed points, namely; $(U,K)=(\pm\infty,0)$ and $(U,K)=(+\infty,+\infty)|_{K=U/2}$. Using the magnetic analog expressed in Eq. (22), we distinguish three phases in the (U,K) plane. The region enclosed by the line *eaf* is the basin of attraction of the fixed point $(U,K)=(+\infty,+\infty)|_{K=U/2}$. This fixed point characterizes a phase with antiferromagneticlike order, i.e., $\langle t_i \rangle > 0$ for all sites of one sublattice and $\langle t_i \rangle < 0$ for the other one. In other words, the sites of one sublattice are predominantly in the state $S_i^z=0$, whereas the sites of the other are in the states $S_i^z=\pm 1$. Consistently, one sublattice has single electronic occupation, while in the other sublattice each site can be either doubly occupied or not occupied at all with equal probability. There is no magnetic order in either of these sublattices. So this phase is a *paramagnetic dimerized-charge insulating* (PDCI) one.

All points belonging to the region $K < U/2$ and outside the line *eaf* are attracted by the fixed point $(+\infty,0)$, which is associated with a phase with $\langle t_i \rangle > 0$ for all sites i. In other words, most of the sites are in the $S_i^z=\pm 1$ states indistinctly, thus describing a *paramagnetic uniform-charge insulating* (PUCI) phase. All points belonging to the region $K > U/2$ and outside the line *eaf*

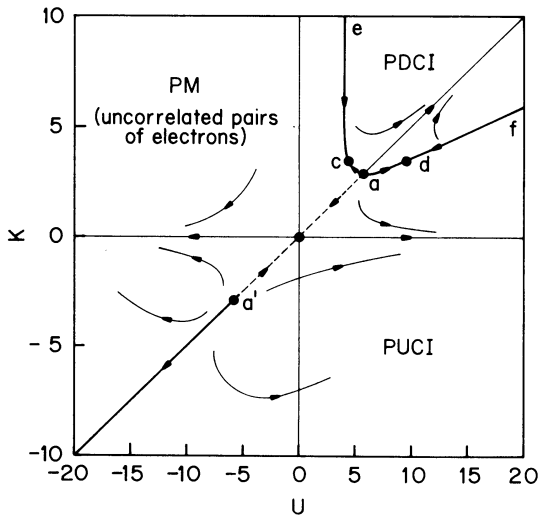

FIG. 3. Flow diagram in the plane (U,K) for $d=2$. The relevant fixed points are labeled a, a', c, and d. The paramagnetic dimerized-charge insulating (PDCI) phase is characterized by the attractor $(U,K)=(+\infty,+\infty)|_{K=U/2}$, while the paramagnetic uniform-charge insulating (PUCI) and the paramagnetic metal (PM) (with uncorrelated pairs of electrons) phases are characterized, respectively, by the attractors $(+\infty,0)$ and $(-\infty,0)$. The line *eaf* is a second-order critical line, while the line $K=U/2$ for $K<K_{a'}$ is a first-order one. The dashed line between points a' and a corresponds to a smooth continuation between the PM and PUCI phases.

are attracted by the fixed point $(-\infty,0)$. This fixed point is associated with a phase with $\langle t_i \rangle < 0$ for all sites i, or equivalently [see Eq. (22)], most of the sites are in the $S_i^z=0$ state. In such situation the electrons are bounded in pairs and one-half of the sites are doubly occupied while the rest of them are empty. Such situation corresponds to a *paramagnetic metallic* (PM) phase in which the carriers are uncorrelated pairs of electrons.

The line af is a second-order transition line between the PUCI and PDCI phases; all points belonging to this line are attracted by the semiunstable fixed point d. The line ae is a second-order line between the PUCI and PM phases; all points belonging to this line are attracted by the semiunstable fixed point c. Both lines join at the critical fixed point a. The fixed points c and d are connected through the unitary transformation $(K,H_t)\rightarrow(K,-H_t)$. Therefore the eigenvalues of the linearized recurrence equations in both fixed points are the same, and consequently the correlation-length critical exponent $\nu_c=\ln b/\ln\lambda_c$ (Refs. 34 and 35) is the same for both transition lines; $\lambda_c=\lambda_d>1$ is the relevant eigenvalue at the fixed point c (d). Along the line $K=U/2$ and $K<K_{a'}$, the ground state of the system is degenerated and we have a first-order transition (two-phase coexistence) between the PM and PUCI phases. This line ends at the critical point a'. Along the line aa' (dashed line in Fig. 2), we have $\langle t_i \rangle=0$, i.e., $\langle S_i^z \rangle=\frac{1}{2}$ for all sites i. All points belonging to this line are attracted by the fixed point (0,0). Such line does not correspond to any phase transition, thus constituting a smooth continuation between the PM and PUCI phases. If we move along the line $K=U/2$ from the PDCI phase, the system undergoes a second-order phase transition at the point a. The correlation-length exponent $\nu_a=\nu_{a'}$ in this case is given by $\nu_a=\ln b/\ln\lambda_a^{(1)}$, where $\lambda_a^{(1)}$ is the eigenvalue of the linearized equations at the point a corresponding to the eigenvector direction $K=U/2$. The crossover exponent is given by $\phi_a=\ln\lambda_a^{(2)}/\ln\lambda_a^{(1)}$, where $\lambda_a^{(2)}$ is the eigenvalue corresponding to the eigenvector direction tangential to the line eaf at the point a. The values of the critical exponents, as well as the location of the fixed points a, c, and d, are listed in Table I for $d=2$ and 3.

Let us now consider the case $J>0$. We are particularly interested in the limit $U\rightarrow\infty$ of the phase diagram because, as we shall see later on, it is closely related to the strong interaction limit of the half-filled-band Hubbard model. For $U\gg1$ the recurrence relations decouple and we find the asymptotic behaviors

$$\begin{aligned} U' &\sim b^{d-1}U \ , \\ K' &\sim f_2(J) \ , \\ J' &\sim f_1(J) \ , \end{aligned} \tag{30}$$

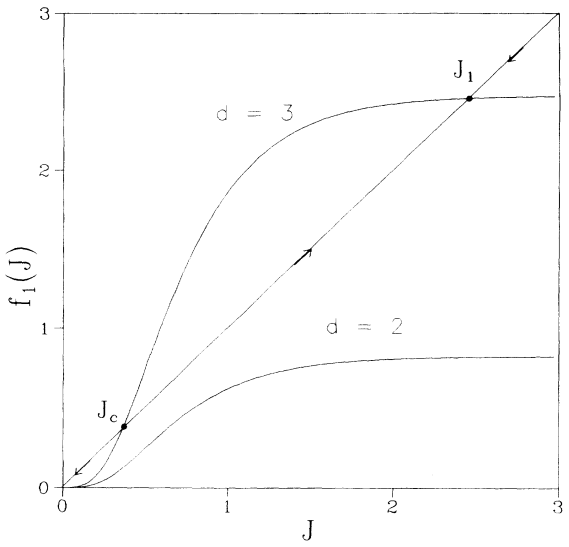

FIG. 4. Asymptotic recurrence relation $J'=f_1(J)$ for the J-K-U model (21) in the limit $U\rightarrow\infty$, for dimensionalities $d=2$ and 3.

and so the only nontrivial recurrence equation is that of the exchange coupling J. This fact can be easily understood if we note that, for $U\gg1$, the states with $S_i^z=\pm1$ for all sites i predominate over all the other states. When we restrict the Hamiltonian (21) to this subspace, the second and third terms become just additive constants which do not affect further ordering, and the Hamiltonian is equivalent to

$$\mathcal{H}\sim -J\sum_{\langle i,j\rangle}\boldsymbol{\sigma}_i\cdot\boldsymbol{\sigma}_j \ , \tag{31}$$

where σ_i^ν, $\nu=x,y,z$, are the Pauli matrices at the site i. The Hamiltonian (31) describes a spin-$\frac{1}{2}$ antiferromagnetic Heisenberg model. The function $f_1(J)$ is depicted in Fig. 4 for $d=2$ and 3.

For $d=2$ the recurrence equations (30) only have trivial fixed points. So the system does not exhibit any phase transition to an ordered state, as expected from (31). For $d=3$ two new fixed points appear, namely, (i) a relevant (critical) fixed point at $J_c=0.353$ and (ii) a stable fixed point at $J_1=2.457$. The critical point J_c corresponds to a second-order phase transition from a paramagnetic phase, characterized by the fixed point $J=0$, to an antiferromagnetic ordered phase $J>J_c$, which is mapped into a finite temperature J_1 fixed point, instead of a zero-temperature ($J=\infty$) one (usual case). Since this shifted fixed point is related to the behavior of the system at zero

TABLE I. Location of the relevant fixed points and critical exponents for $J=0$ and $K>0$. The location of the fixed point a' is $U_{a'}=-U_a$, $K_{a'}=-K_a$, and the corresponding critical exponent is $\nu_{a'}=\nu_a$.

d	U_a	K_a	U_c	K_c	U_d	K_d	ν_a	ν_c	ϕ_a
2	5.77	2.89	4.38	3.48	9.54	K_c	1.35	1.22	0.17
3	2.83	1.42	2.61	8.68	32.10	K_c	1.08	0.55	1.54

temperature, such shift is probably due to the approximation (17).[36] At zero temperature such approximation might be a rough one, and therefore spurious results could appear at very temperatures. In fact, very good results have been found in other models for a wide range of temperatures.[25,26]

As the dimensionality d decreases, the fixed points J_c and J_1 approach each other and merge into a marginal fixed point at the lower critical dimension $d_c \approx 2.41$ [at $d=d_c$, $f_1(J)$ becomes tangential to $J'=J$]. The correlation-length exponent for this transition is given by $\nu_a = \ln b / \ln \lambda_J$, where

$$\lambda_J = \left. \frac{df_1}{dJ} \right|_{J=J_c} .$$

In Table II we compare our $d=3$ results for J_c and ν_J with those obtained by high-temperature series expansions for the antiferromagnetic Heisenberg model in some Bravais lattices.[37]

For lower values of U, the $d=3$ phase diagram is very similar to the RG phase diagram of the $d=2$ ferromagnetic BEG model, with and appropriate change of signs in the coupling parameters and the magnetic order parameter replaced by the z component of the staggered magnetization.[31] Since in the present work we are mainly interested in those characteristics of the complete phase diagram (U,K,J,I,t,D) related to the t-hopping term and since the fixed points which determine such features are those located in the $U \gg 1$ region (see Sec. IV C), we will give here only a brief description of the phase diagram (U,K,J) for intermediate values of U.

We find a second-order transition surface from a paramagnetic (PUCI) to an *antiferromagnetic insulating* (AFI) phase. For $U \gg 1$ this surface becomes parallel to the $J=0$ plane at a height J_c. This critical surface is associated to the fixed point $(U,K,J)=(+\infty, K_c, J_c)$, where $K_c \equiv f_2(J_c) = -0.001$. For $U<0$ the PM and AFI phases are separated by a first-order transition surface. Such surface is associated with the first-order fixed point $(-\infty, -\infty, J_1)|_{K=U/2}$. The relevant eigenvalue for such a fixed point fulfills the Nienhuis condition $\lambda = b^d$.[38] Both surfaces (first and second order) join smoothly at a line of tricritical points. Such line is associated with the tricritical fixed point $(U_T,K_T,J_T) = (-2.27, -0.16, 0.79)$.[39] For this tricritical point we find two relevant eigenvalues $\lambda_T^{(1)}$ and $\lambda_T^{(2)}$, with $\lambda_T^{(1)} > \lambda_T^{(2)} > 1$, and a third eigenvalue $\lambda_T^{(3)} < 1$. The eigenvector directions associated with $\lambda_T^{(2)}$ and $\lambda_T^{(3)}$ are tangential to the transition surface, while that corresponding to $\lambda_T^{(1)}$ is transversal to the transition surface. The eigenvector direction associated with $\lambda_T^{(3)}$ is tangential to the tricritical line. The tricritical exponents are given by[40] $\nu_T = \ln b / \ln \lambda_T^{(1)}$ and $\phi_T = \ln \lambda_T^{(2)} / \ln \lambda_T^{(1)}$. We find $\nu_T = 0.40$ and $\phi_T = 0.21$ (no other numbers are available in the literature for comparison). Besides these two magnetic transition surfaces, there is a first-order surface associated with the fixed point $(U,K,J)=(-\infty,-\infty,0)|_{K=U/2}$, which constitutes an extension of the first-order line between the PM and PUCI phases shown in Fig. 3. This fixed point also satisfies the Nienhuis conditions for a first-order one. The first-order surface between the PM and PUCI phases ends at an isolated critical line whose points are all attracted by the critical fixed point a (see Fig. 3). The three transition surfaces join along a critical-end line associated with the fixed point $(U,K,J)=(-\infty,-\infty,J_c)|_{K=U/2}$. This fixed point has two relevant eigenvalues: $\lambda_1 = b^{\nu_J}$ and $\lambda_2 = b^d$. Moreover, the two first-order surfaces have the same slope at such a line. This features provide the RG characterization of critical-end point behavior. The three critical lines (critical end, tricritical, and isolated critical) join at a fully unstable multicritical fixed point $(U,K,J)=(-2.66, -0.75, 0.59)$.

As an example, we show the section of the phase diagram with the $K=0$ plane in Fig. 5. The location of the tricritical point T_0 for $K=0$ is $(U,J)=(-2.22, 0.86)$.

Another feature which appears for $K>0$ and $U>0$ is the paraboloidlike extension of the critical line *(eaf* line) appearing in Fig. 3. Most of the points of this surface are attracted either by point c or by point d of Fig. 3; at the frontier of these two sets of points, a critical line exists whose points are attracted by point a of Fig. 3.

TABLE II. Critical coupling and critical exponent for the antiferromagnetic J-K-U model (21) in a hierarchical lattice ($U \gg 1$), compared with those obtained through high-temperature series expansions for the antiferromagnetic Heisenberg model in the face-centered (fcc), body-centered (bcc), and simple cubic (sc) lattices (Ref. 37).

	ν_J		J_c
J-K-U model ($U \gg 1$) (RG)	1.241		0.353
Heisenberg model (series)	0.753	fcc	0.232
		bcc	0.357
		sc	0.520

B. I-K-U model ($t=D=J=0$)

The Hamiltonian (19) reduces in this case to

$$\mathcal{H}_{I\text{-}K\text{-}U} = -I \sum_{\langle i,j \rangle} [\rho_i^z \rho_j^z - (\rho_i^x \rho_j^x + \rho_i^y \rho_j^y)] - K \sum_{\langle i,j \rangle} (S_i^z)^2 (S_j^z)^2 + \tfrac{1}{2} U \sum_i (S_i^z)^2 . \quad (32)$$

By using the canonical transformation (7), the Hamiltonian (32) can be mapped into the Hamiltonian (21) with a new set of coupling constants, namely [see Eq. (20)],

$$\tfrac{1}{2}U \rightarrow 2K - \tfrac{1}{2}U , \qquad I \rightarrow J . \quad (33)$$

Consequently, the phase diagram corresponding to the Hamiltonian (32) can be obtained from the phase diagram of the J-K-U model by means of the transformation (33). This correspondence between the two phase diagrams is exactly recovered by our recurrence equation (29). Since $(S_i^z)^2 = 1 - (\rho_i^z)^2$, the Hamiltonian (32) can be easily ex-

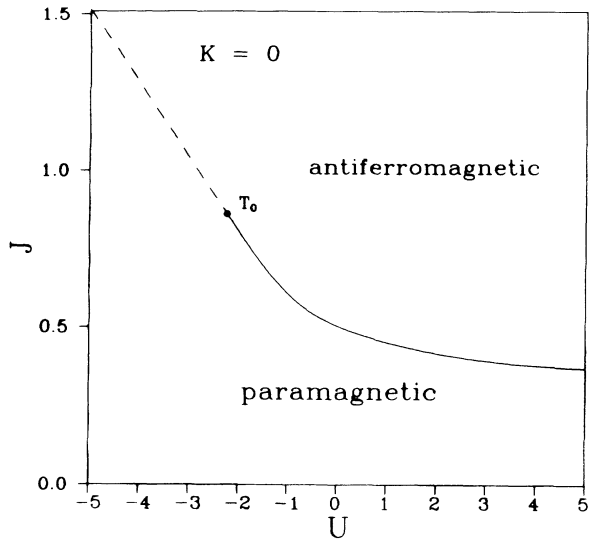

FIG. 5. Phase diagram of the J-K-U model ($J>0$) for $K=0$ and in $d=3$. The solid line is a second-order critical line, while the dashed line is a first-order one. Both lines join at the tricritical point T_0.

pressed only in terms of charge operators. In particular, for $U \ll -1$ electron-pair formation is favored and the Hamiltonian (32) can be seen as a gas of bosons with hard cores and long-range interactions. Such bosons are (on site) bounded pairs of electrons. In the limit $U \to -\infty$, which is mapped through (33) into the $U \to +\infty$ limit of the J-K-U model (21), the only term that contributes in the Hamiltonian (32) is the first one. This term can be obtained by perturbation theory from the original Hubbard Hamiltonian in the limit $U \to -\infty$.[41] From Eqs. (10) we see that in this case the antiferromagnetic order in the z direction of the J-K-U model is associated with the nonvanishing order parameter

$$\frac{1}{\mathcal{N}} \sum_i \langle \rho_i^z \rangle \exp(i\mathbf{Q}\cdot\mathbf{R}_i) = \frac{1}{\mathcal{N}} \sum_{\mathbf{k},\sigma} \langle c^\dagger_{\mathbf{k},\sigma} c_{\mathbf{k}+\mathbf{Q},\sigma} \rangle \ , \quad (34)$$

where the sum over $\mathbf{k}$ runs over the first Brillouin zone. Such state corresponds to a charge-density-wave (CDW) ordered phase. A nonvanishing x-y plane antiferromagnetic order parameter will imply a nonvanishing value for

$$\frac{1}{\mathcal{N}} \sum_i \langle c^\dagger_{i,\uparrow} c^\dagger_{i,\downarrow} \rangle = \frac{1}{\mathcal{N}} \sum_{\mathbf{k}} \langle c^\dagger_{\mathbf{k},\uparrow} c^\dagger_{-\mathbf{k},\downarrow} \rangle \ , \quad (35)$$

which corresponds to singlet superconductivity (SS). If both order parameters (34) and (35) are zero, then the pairs are completely uncorrelated (PM phase) if U is negative enough or there are no pairs (PUCI phase) if U is high enough. In the second case the states with $\rho_i^z=0$ predominate, while in the former the states which predominate are the $\rho_i^z=\pm 1$ ones. By using Eq. (33) we obtain for the $d=3$ phase diagram corresponding to the Hamiltonian (32), in the region $U \ll -1$ and $I>0$, a second-order critical surface; on one side of it we have the PM phase, while on the other side we have the mixed CDW-SS phase. This surface is associated with the fixed point $(U,K,I)=(-\infty,K_c,I_c)$, where $I_c=J_c$ and the correlation-length exponent is $\nu_I=\nu_J$ (J_c and ν_J were defined in Sec. IV A). The mixed phase is associated with the fixed point $(-\infty,K_1,I_1)$, with $I_1=J_1$, and the PM phase is associated with the fixed point $(-\infty,0,0)$. The rest of the phase diagram can be similarly obtained from the results of Sec. IV A.

C. Half-filled-band Hubbard model

We now consider the section of the phase diagram with the (U,t) plane (which is not invariant under the RG transformation), i.e., $I=J=K=D=0$, for both signs of U (see Ref. 23). This case corresponds to the half-filled-band Hubbard model (2).

In $d=1$ our RG yields no phase transition for any value of $U \neq 0$, as expected.[15] All points in the (U,t) plane are attracted by the $t=0$ line, which is a line of fixed points. Points with $U>0$ are attracted by points in the positive-U axis with $U \gg 1$, which characterizes an *insulating* phase. Points with $U<0$ are attracted by points in the negative-U axis with $|U| \gg 1$. In this situation the electrons are bounded in pairs; for $d=1$ there is no correlation between such pairs. So the system behaves as a metal whose charge carriers are bounded pairs. All points in the t axis are attracted by the fixed point $(U,K,J,I,t,D)=(0,0,0,0,0,0)$. For $U=0$ we have a pure tight-binding system (free particles), and in this case the rescaling involved in the decimation procedure reduces, at every RG step, the bandwidth (proportional to the hopping parameter t), because it eliminates the short-wavelength states. Consequently, $t \to 0$, and the fixed point (0,0,0,0,0,0) characterizes, in this case, a normal metallic phase.

For $d>1$ and $U>0$, all points are attracted into the parameter subspace $t=D=I=0$ with $U \to \infty$. This subspace was already analyzed in Sec. IV A, and we saw that in the $U \to \infty$ limit the thermodynamical properties of the system are entirely determined by the Heisenberg Hamiltonian (31). Therefore we conclude that the ground state of the half-filled-band Hubbard model is always insulating and antiferromagnetic; i.e., no Mott transition is observed for the ground state at $U \neq 0$. This results satisfy Lieb's theorem.[42] For $d>1$ and $U<0$, all points are attracted into the subspace $t=D=J=0$ with $U \ll -1$. Therefore, for $U<0$, the ground state of the system is composed by a gas of bosons (bounded pairs of electrons) with hard cores and long-range interactions (see Sec. IV B).

In $d=2$ we find, for the phase diagram, structure which is similar to that for $d=1$. All points in the $U=0$ axis are attracted by the fixed point (0,0,0,0,0,0). Hence, for $U=0$, the system is a *normal metal*. For $U>0$ all points are attracted by the fixed point $(+\infty,0,0,0,0,0)$, which corresponds to a PUCI phase, as we have seen in Sec. IV A. Since, for $U \to \infty$, the electrons are localized, the system is a paramagnetic insulator for any value of $U>0$ and finite temperatures. These results are in agreement with previous ones obtained by a different RG technique[22] and by Monte Carlo calculations.[18] For $U<0$ all points are attracted by the fixed point $(-\infty,0,0,0,0,0)$. As we have seen in Sec. IV B, in this case there is neither

superconductivity nor charge-density waves, and the system is in a PM phase (uncorrelated pairs of electrons).

For $d=3$ the calculated phase diagram is shown in Fig. 6, where, instead of the (U,t) variables, we have used the more appropriate ones, namely; $1/t$ (dimensionless temperature) and U/t. For $U/t>0$ the system is always an insulator and there is a second-order transition line. Points below this line are associated with the antiferromagnetic fixed point $(U,K,J,I,t,D)=(+\infty,K_1,J_1,0,0,0)$, while points above this line are associated with the paramagnetic fixed point $(+\infty,0,0,0,0,0)$. The critical line is associated with the critical fixed point $(+\infty,K_c,J_c,0,0,0)$, and so it describes a second-order para-antiferromagnetic phase transition; the corresponding correlation-length exponent ν_J is given in Table II.

For $U/t<0$ there is a second-order phase transition from the PM phase at high temperature to the mixed phase CDW-SS (see Sec. IV B). The coexistence of CDW and SS in the negative-U Hubbard model is a particular degeneracy of the half-filled-band case. The degeneracy is removed in the non-half-filled-band case.[41,43] The corresponding transition line is associated with the critical fixed point $(U,K,J,I,t,D)=(-\infty,K_c,0,I_c,0,0)$, and the correlation-length exponent for such transition is $\nu_I=\nu_J$. The two critical lines for $U/t>0$ and $U/t<0$ meet at a point $1/t_c\neq 0$ in the $U/t=0$ axis (pure tight-binding limit). For $U/t=0$ and $1/t>1/t_c$, all the points are attracted by the (0,0,0,0,0,0) fixed point; i.e., that region corresponds to a normal metallic phase. For $1/t<1/t_c$ we found an anomalous behavior in the renormalization flow. All the points are attracted by limit cycles of order 2 rather than being attracted by normal fixed points. More precisely, the points are attracted by one or the other of two different cycles related among them through the transformation $(t,D)\rightarrow(-t,-D)$. The basins of attraction of these two cycles alternatively appear along the $U/t=0$ axis in the region $0<1/t<1/t_c$. At the time the physical meaning (if it exists) of these limit cycles is not clear, but they might be related to the fractal character of the hierarchical lattice. The general structure of the limit cycles and its possible relation with fractality is discussed in Ref. 23. This anomalous behavior disappears $(1/t_c\rightarrow 0)$, for dimensionalities $d<d_c$, where $d_c\sim 2.41$, which is the same value found in Sec. IV A for the lower critical dimension of the para-antiferromagnetic transition for $U/t\gg 1$. This suggests that the whole critical line disappears at $d=d_c$.

D. Hubbard model with biquadratic interactions

We now consider the section $I=J=D=0$ of the phase diagram in $d=2$ and 3 (the $d=1$ case presents no novelty with respect to the $d=1$ case of Sec. IV C). In this case the Hamiltonian (19) describes a half-filled-band Hubbard model with biquadratic interactions between electrons in nearest-neighboring sites:

$$\mathcal{H}=t\sum_{\langle i,j\rangle,\sigma}(c^{\dagger}_{i,\sigma}c_{j,\sigma}+c^{\dagger}_{j,\sigma}c_{i,\sigma}) +\tfrac{1}{2}U\sum_i(n_{i,\uparrow}-n_{i,\downarrow})^2-K\sum_{\langle i,j\rangle}(S^z_i)^2(S^z_j)^2 . \quad (36)$$

We first consider the $d=2$ case. The sections of this phase diagram with the planes $t=0$ and $K=0$ were already analyzed in Secs. IV A and IV B, respectively. We now discuss the section of this phase diagram with the plane $K=U/2$. As we have seen in Sec. III, the subspace $I=J$ and $K=U/2$ of the complete (U,K,J,I,t,D) parameter space is invariant under the RG transformation. In particular, the $I=J=0$ points flow into $I=J\neq 0$ ones. The phase diagram we obtain for $K=U/2$ is shown in Fig. 7. The normal metallic phase is associated with the fixed point $(U,K,J,I,t,D)=(0,0,0,0,0,0)$. For $U<0$ there is a coexistence region of the PUCI phase [associated with the fixed point $(+\infty,0,0,0,0,0)$], and the PM phase [associated with the fixed point $(-\infty,0,0,0,0,0)$]. This region is attracted by the first-order fixed point $(-\infty,-\infty,0,0,0,0)|_{K=U/2}$ and ends at the critical line $a'b'$ (Fig. 7), which is associated with the fixed point $(U_{a'},K_{a'},0,0,0,0)$. For $U>0$ there is a PDCI phase, which is associated with the fixed point

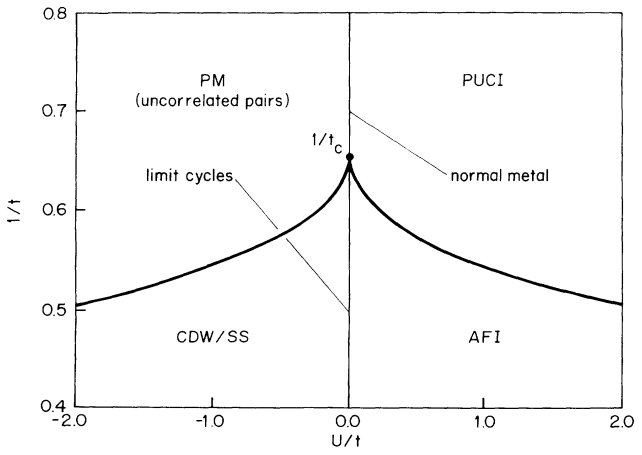

FIG. 6. Phase diagram of the half-filled-band Hubbard model in $d=3$ ($1/t$ is the dimensionless temperature).

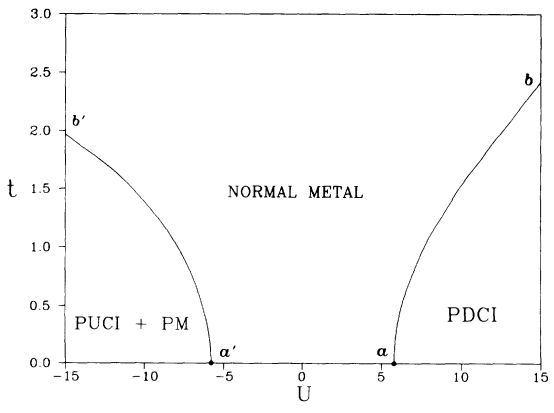

FIG. 7. Phase diagram for the $d=2$ half-filled-band Hubbard model with biquadratic interactions for $K=U/2$. There is a coexistence region of the PUCI and PM phases (uncorrelated pairs of electrons).

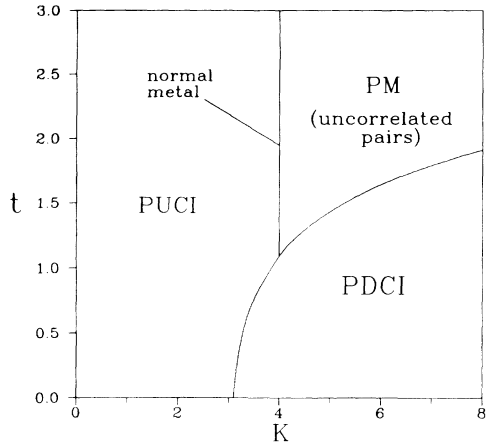

FIG. 8. Phase diagram for the $d=2$ half-filled-band Hubbard model with biquadratic interactions for constant $U=8$.

$(+\infty,+\infty,0,0,0,0)|_{K=U/2}$. The line ab (Fig. 7) corresponds to a second-order metal-insulator phase transition, and it is associated with the relevant fixed point $(U_a,K_a,0,0,0,0)$ (see Table I for the location of the relevant fixed points).

Let us now consider the rest of the phase diagram in the space (U,K,t), i.e., for $K\neq U/2$. For $K>0$ and $U>0$, there is a critical surface whose sections with the planes $t=0$ and $K=U/2$ are shown in Figs. 3 and 7, respectively. For $K>U/2$ this surface is associated with the fixed point $(U_d,K_d,0,0,0,0)$, while for $K<U/2$ it is associated with the fixed point $(U_c,K_c,0,0,0,0)$. For $K>U/2$ this surface describes a second-order metal-insulator phase transition separating the PDCI and PM phases. The PM phase extends over the whole region $K>U/2$, outside the region enclosed by the critical surface. For $K<U/2$ the surface corresponds to a second-order phase transition separating the PDCI and PUCI phases. All points with $K<U/2$, outside the region enclosed by the critical surface, belong to the PUCI phase.

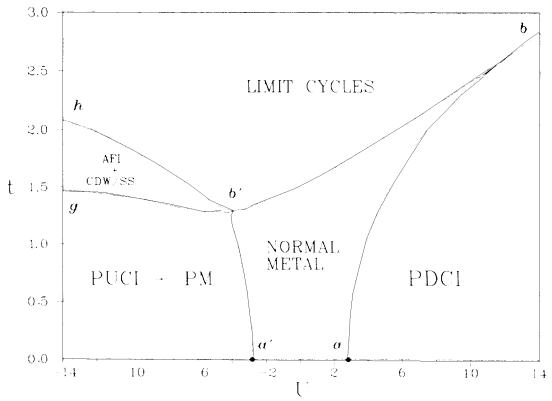

FIG. 9. Phase diagram for the $d=3$ half-filled-band Hubbard model with biquadratic interactions for $K=U/2$. See text for details.

In Fig. 8 we show a section of the phase diagram for $K>0$ with a constant-U plane $(U=8)$.

For $K<0$ and $U<0$, the PUCI and PM phases are separated by the first-order surface shown in Fig. 7, where the system undergoes a discontinuous metal-insulator transition. This surface ends at the isolated critical line $a'b'$. Outside this surface and for $K=U/2$,

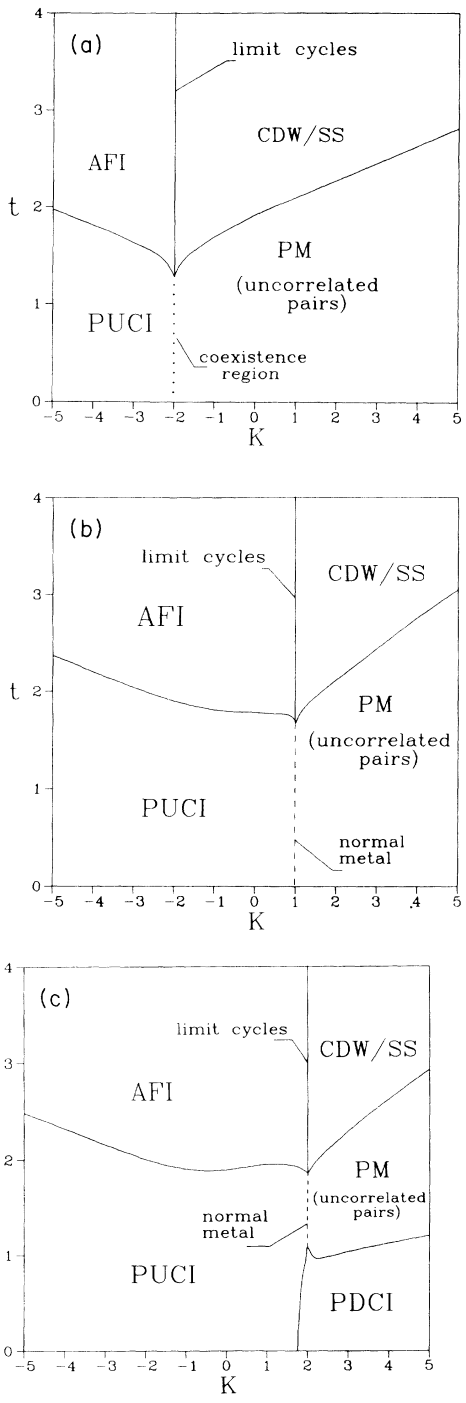

FIG. 10. Phase diagram for the $d=3$ half-filled-band Hubbard model with biquadratic interactions for constant U. See text for details. (a) $U=-4$, (b) $U=2$, and (c) $U=4$.

the system changes smoothly (i.e., without a phase transition) from the PM phase ($K > U/2$) to the PUCI phase ($K < U/2$), passing through a normal metallic state at $K = U/2$, where the pairs break.

Finally, we consider the phase diagram for $d=3$, whose section with the plane $K = U/2$ is shown in Fig. 9. For low values of the parameter t, the phase diagram shows the same qualitative structure as the $d=2$. For higher values of t, new features appear. First, we find that the limit cycles already observed for $U=K=0$ extend over the plane $K = U/2$ for t above the line $hb'b$. The basins of attraction of the two cycles appear as alternated fringes of complex shape. The appearance of limit cycles occurs only for $K = U/2$. Second, between the coexistence region of the PUCI and PM phases and the limit cycles region, a new region appears; two ordered phases (namely, AFI and CDW-SS) coexist. Such region is associated with the fixed point $(-\infty, K_1, J_1, I_1, 0, 0)$. This coexistence can be understood if we note that for $K = U/2$ the second and third terms of the Hamiltonian (36) can be rewritten for the hierarchical lattice as

$$\tfrac{1}{4}U \sum_{\langle i,j \rangle} [(S_i^z)^2 - (S_j^z)^2]^2 .$$

For $U \ll -1$ the configurations that predominate are those for which $S_i^z = 0$ or those for which $S_i^z = \pm 1$ for all sites i. Both types of configurations (i.e., $S_i^z = 0$ or $S_i^z = \pm 1$) are degenerate, and so they have the same occurrence probability. For low values of t, this degeneracy leads to the coexistence of the two disordered phases (PM + PUCI) that we have already seen for $d=2$. As the parameter t increases, each one these phases undergoes a second-order phase transition to the corresponding ordered phase at the line gb'. This degeneracy could also be related to the occurrence of the fixed cycles for $K = U/2$.

For $K < U/2$ there is a second-order transition surface separating the PUCI phase (low values of t) and the AFI phase (high values of t); this surface is associated with the fixed point $(U, K, J, I, t, D) = (+\infty, K_c, J_c, 0, 0, 0)$. For $K > U/2$ there is a second-order surface separating the PM phase (low values of t) and the CDW-SS mixed phase (high values of t); this surface is associated with the fixed point $(-\infty, K_c, 0, I_c, 0, 0)$. Both $K < U/2$ and $K > U/2$ second-order surfaces join at the line $gb'b$ of the plane $K = U/2$ (see Fig. 9). The AFI and CDW-SS phases are separated, on the $K = U/2$ plane, by limit cycles excepting a small region (enclosed by $gb'h$ in Fig. 9) where these two phases coexist. In Fig. 10 we show some sections of the phase diagram with constant-U planes for typical values of U.

V. CONCLUSIONS AND REMARKS

We have discussed a very general Hamiltonian [Eq. (24)] which contains the Hubbard one as a particular case. The general Hamiltonian remains invariant under a specific real-space RG scheme in which the d-dimensional Bravais lattices are replaced by d-dimensional hierarchical ones. This Hamiltonian, besides including the Hubbard Hamiltonian as a particular case, contains several interaction terms that allow the study of the critical properties of a great variety of interacting fermionic systems; indeed, these terms account for charge fluctuation and magnetic order, as well as hopping. The complete phase diagram presented in Sec. IV for the half-filled-band Hamiltonian (19) shows the richness of this model. Among other applications of the general Hamiltonian (24), the most interesting seems to be the study of high-T_c superconducting compounds. This Hamiltonian contains many of the basic interactions that have been proposed to explain this phenomenon. Indeed, we have shown that adding a nearest-neighbor interaction term to the half-filled-band Hubbard Hamiltonian [like the biquadratic term in Hamiltonian (36)] can cause a superconducting phase to appear, *even for repulsive intrasite interactions* (see Fig. 10). The use of the generalized Hubbard Hamiltonian [Eq. (24)] together with the RG formalism appears as a powerful tool to analyze the combined effects of different types of interactions. The numerical results in $d=1$ and 2 for the Hubbard model are encouraging in this sense, since they reproduce the expected qualitative aspects of the corresponding phase diagrams. In $d=3$ the method works well in the strong interaction region $|U/t| \gg 1$. For $|U/t| \ll 1$ the appearance of limit cycles makes the applicability of this method questionable in the sense that the results for Bravais lattices might be quite different from those in hierarchical lattices (see also Ref. 23). The fact that this phenomenon occurs only for some region of the $K = U/2$ subspace suggests that it could be due to a particular degeneracy of the ground state of the hierarchical lattice. Indeed, limit cycles of order 2 in the RG flow have been encountered for Ising systems with competing interactions, where such behavior reflects certain degeneracies of the ground state of the model.[44] Excepting for this $|U/t| \ll 1$ region, the results herein obtained seem to be encouraging toward the final understanding of this complex quantum many-body problem. Further developments, in particular the non-half-filled-band case, are planned to be presented elsewhere.

ACKNOWLEDGMENTS

We wish to thank D. Prato, E. M. F. Curado, R. Maynard, and L. M. Falicov for fruitful discussions and suggestions. Two of us (S.A.C. and F.A.T.) thank CNPq (Brazil) for financial support.

[1] J. Hubbard, Proc. R. Soc. London A **276**, 238 (1963).
[2] Y. Nagaoka, Phys. Rev. **147**, 392 (1966).
[3] W. F. Brinkman and T. M. Rice, Phys. Rev. B **2**, 4302 (1970).
[4] M. Cyrot, J. Phys. (Paris) **33**, 125 (1972).
[5] *Electron Correlations and Magnetism in Narrow Band Systems*, edited by T. Moriya (Springer, New York, 1981).
[6] F. C. Zhang and T. M. Rice, Phys. Rev. B **37**, 3759 (1988).
[7] P. W. Anderson, Science **235**, 1196 (1987).

[8]V. J. Emery, Phys. Rev. Lett. **58**, 2794 (1987).
[9]M. Cyrot, Solid State Commun. **62**, 821 (1987); **63**, 1015 (1987).
[10]C. R. Proetto and L. M. Falicov, Phys. Rev. B **15**, 1754 (1988).
[11]J. R. Schrieffer, X. G. Wen, and S. C. Zhang, Phys. Rev. Lett. **60**, 944 (1988).
[12]Wei-ming Que and G. Kirczenow, Z. Phys. B **73**, 425 (1989).
[13]B. I. Shraiman and E. D. Siggia, Phys. Rev. Lett. **60**, 740 (1988).
[14]R. Micnas, J. Ranninger, and S. Robaszkiewicz, J. Phys. C **21**, L145 (1988).
[15]E. H. Lieb and F. Y. Wu, Phys. Rev. Lett. **20**, 1445 (1968).
[16]D. Penn, Phys. Rev. **142**, 350 (1966).
[17]M. C. Gutzwiller, Phys. Rev. **137**, A1726 (1965).
[18]J. Hirsch, Phys. Rev. B **31**, 4403 (1985).
[19]J. Hirsch, Phys. Rev. B **35**, 1851 (1987).
[20]C. Vanderzande and A. L. Stella, J. Phys. C **17**, 2075 (1984).
[21]H. Takano and M. Suzuki, Physica **109A**, 618 (1981).
[22]C. Vanderzande, J. Phys. A **18**, 889 (1985).
[23]S. A. Cannas, F. A. Tamarit, and C. Tsallis, Solid State Commun. **78**, 685 (1991).
[24]A. O. Caride, C. Tsallis, and S. I. Zanette, Phys. Rev. Lett. **51**, 145 (1983); **51**, 616 (1983).
[25]A. M. Mariz, C. Tsallis, and A. O. Caride, J. Phys. C **18**, 4189 (1985).
[26]H. Takano and M. Suzuki, J. Stat. Phys. **26**, 635 (1981).
[27]H. Shiba, Prog. Theor. Phys. **48**, 2171 (1972).
[28]C. Castellani, C. DiCastro, D. Feinberg, and J. Ranninger, Phys. Rev. Lett. **43**, 1957 (1979).
[29]J. W. Essam and C. Tsallis, J. Phys. A **19**, 409 (1986). A. C. N. de Magalhães and J. W. Essam, *ibid.* **19**, 1955 (1986); **22**, 2549 (1988).
[30]B. Blume, V. J. Emery, and R. B. Griffiths, Phys. Rev. A **4**, 1071 (1971).
[31]A. N. Berker and M. Wortis, Phys. Rev. B **14**, 4946 (1976).
[32]J. B. Marston and I. Affleck, Phys. Rev. B **39**, 11 538 (1989).
[33]R. B. Griffiths, Physica **33**, 689 (1967).
[34]Th. Niemeijer and J. M. J van Leeuwen, in *Phase Transitions and Critical Phenomena,* edited by C. Domb and M. S. Green (Academic, New York, 1976), Vol. 6.
[35]S. Ma, *Modern Theory of Critical Phenomena* (Benjamin, New York, 1976).
[36]The appearance of shifted fixed points of this kind was encountered by other authors, in the same approximation applied to the anisotropic (ferromagnetic) Heisenberg model in $d=3$ (see Ref. 26).
[37]G. S. Rushbrooke, G. A. Baker, Jr., and P. J. Wood, in *Phase Transitions and Critical Phenomena* (Ref. 34), Vol. 3.
[38]B. Nienhuis and M. Nauenberg, Phys. Rev. Lett. **35**, 477 (1975).
[39]B. Nienhuis and M. Nauenberg, Phys. Rev. B **13**, 2021 (1976).
[40]P. Pfeuty and G. Toulouse, *Introduction to the Renormalization Group and to Critical Phenomena* (Wiley, New York, 1977).
[41]V. J. Emery, Phys. Rev. B **14**, 2989 (1976).
[42]E. H. Lieb, Phys. Rev. Lett. **62**, 1201 (1989).
[43]R. Micnas *et al.*, Phys. Rev. B **37**, 9410 (1988).
[44]P. M. C. Oliveira, J. Phys. (Paris) **47**, 1107 (1986).